

Cite this article as: Wang Fuqiang, Chen Jian, Wang Kunjie, et al. Thermo-structural Simulation and Ablation Behavior of 3D C/C Composites Throat in Solid Rocket Motor[J]. Rare Metal Materials and Engineering, 2022, 51(03): 873-880.

ARTICLE

Thermo-structural Simulation and Ablation Behavior of 3D C/C Composites Throat in Solid Rocket Motor

Wang Fuqiang^{1,2}, Chen Jian¹, Wang Kunjie², Cui Hong², Ji Alin², Xie Dong², Bai Yang²

¹ School of Materials Science and Chemical Engineering, Xi'an Technological University, Xi'an 710021, China; ² Xi'an Aerospace Composites Institute, Xi'an 710025, China

Abstract: The heat transfer coefficient, temperature distribution, and stress distribution of 3D carbon/carbon (C/C) composite solid rocket motor (SRM) throat at the thermal equilibrium state were calculated through the comprehensive thermo-structural simulation, and SRM used the tri-component propellant of ammonium perchlorate/hydroxyl-terminated polybutadiene/Al under the condition of 6.5 MPa for long run of 20, 60, and 95 s. The analysis of ablation behavior and mechanism of different throat regions was also conducted according to the simulation results. The results show that the temperature at throat convergent zone is the highest due to the thermochemical ablation between the oxidation components (H_2O , CO_2 , H_2) and the surface carbon. The central throat zone has the maximum heat transfer coefficient with relatively high temperature. The ablation in the central throat zone is the most severe due to the stress of inner surface, including the gas thermochemical ablation, high-speed-flow mechanical denudation, and particle erosion. The central throat surface has small grooves or cracks, and the throat tends to decompose due to the stress and oxidation. The stress and temperature of throat exit zone are decreased, and the ablation rate is obviously reduced. The throat ablation mechanism is the combination effect of thermochemical ablation of oxidation components and the carbon influenced by the stress and temperature, flow mechanical denudation, and Al_2O_3 particle erosion.

Key words: throat; thermo-structural simulation; ablation behavior; C/C; solid rocket motor

The nozzle throat is a key component for the solid rocket motor (SRM), because the nozzle throat ablation reduces the motor specific impulse and changes the motor thrust profile^[1-3]. For accurate prediction and precious thrust control, it is necessary to control the ablation of throat material. However, the throat ablation is usually caused by the complex interactions under the extremely harsh conditions of high temperature, high pressure, high-velocity gas flow, chemically aggressive gas, and the mechanical action by particles. The common nozzle throat materials are the pyrolytic graphite, tungsten (or refractory metals), carbon-phenolic, and carbon/carbon (C/C) composites^[4-7]. The C/C composites are a structural and functional coupling material, which is suitable for nozzle application due to the superior behavior in high heat transfer regions^[8-11].

Predicting the nozzle throat erosion is very important for SRM nozzle design, which becomes more and more critical

with increasing the motor scale, because the firing duration is proportional to the motor size, and the change in the nozzle throat area at the same regression depth is inversely proportional to the square of the motor size. Thus, the investigation on the ablation behavior, thermo-structural analysis, and structural design of throat components are important^[12-17]. The C/C throat ablation using the oxyacetylene flame, plasma torch, electric arc, and other oxyfuel flame has been studied, but the results cannot be applied under the comprehensive conditions of high temperature, high pressure, high-velocity gas, and the gas with fusion particles for the large-scale SRM^[18-22]. In this research, the ablation behavior of 3D C/C composite throat was investigated in full-scale SRM for long duration. The throat ablation behavior based on the simulation results was analyzed. The ablation mechanism of 3D C/C throat at thermomechanical condition was discussed. The ablation rate of nozzle throat in SRM for long duration was

Received date: March 10, 2021

Foundation item: China Advance Research Item (30506070503)

Corresponding author: Chen Jian, Ph. D., Professor, School of Materials Science and Chemical Engineering, Xi'an Technological University, Xi'an 710021, P. R. China, Tel: 0086-29-86173054, E-mail: chenjian@xatu.edu.cn

Copyright © 2022, Northwest Institute for Nonferrous Metal Research. Published by Science Press. All rights reserved.

obtained. This research may provide guidance for the modeling of nozzle throat ablation, the throat material modification, and the nozzle design.

1 Experiment

The C/C composites were made by unidirectional carbon cloth and polyacrylonitrile-based carbon fiber yarns. The carbon cloth was piled up layer by layer until it reached the designed height, and then the carbon fiber yarns penetrated the layered carbon cloth, as shown in Fig.1. The C/C composites were then densified with coal-tar pitch by high isostatic pressing carbonization. The density and open porosity of C/C composites were 1.95 g/cm³ and 3.2%, respectively. The degree of graphitization is about 80% through X-ray diffraction (XRD) analysis. Fig.2 shows the microstructures of C/C composites. A few voids and cracks exist, and the void size is less than 50 μm. The width and length of cracks are less than 10 and 100 μm, respectively. It can be seen that the cracks are blocked by the carbon cloth or the carbon fiber yarns. The bulk C/C composites were machined to obtain the

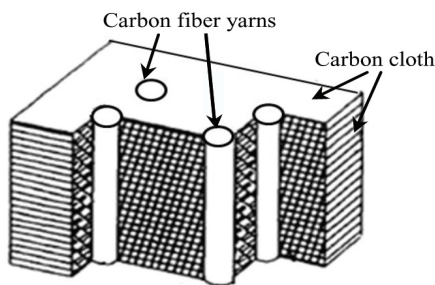


Fig.1 Schematic diagram of 3D C/C composites

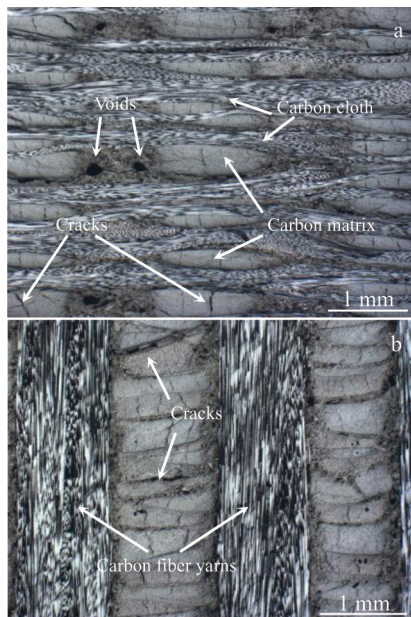


Fig.2 Microstructures of layered carbon cloth (a) and carbon fiber yarns (b) in 3D C/C composites

throat. The flame was parallel along z direction of each throat. The throat diameter before and after firing was measured by the micrometer. The average linear ablation rate of the throat could be calculated by Eq.(1), as follows:

$$r_c = \frac{d_1 - d_2}{t} \quad (1)$$

where r_c is the linear ablation rate; d_1 and d_2 are the average diameters of central throat zone before and after ablation, respectively; t is burning duration.

Fig. 3 shows the schematic diagram of SRM. The microstructures of different zones in the throat were observed by a scanning electron microscope (SEM, JSM-6460).

The propellant for SRM tests was 69wt% ammonium perchlorate/13wt% hydroxyl-terminated polybutadiene/18wt% aluminum (AP/HTPB/Al). The flame temperature was 3500 K. The gas temperature at the throat was determined through the equilibrium calculations based on the propellant. The ablation duration was 20, 60, and 95 s and the stress was 6.5 MPa. The test parameters are shown in Table 1.

2 Results and Discussion

2.1 Thermo-structural simulation

2.1.1 Boundary condition

The convective heat transfer and temperature distribution were simulated by the computational fluid mechanics in FLUENT software. The stress distribution was simulated by the finite element analysis in ANSYS software. The boundary conditions should be specified to complete the theoretical model. The solid and gas boundaries connect at the interface. The mass flux and energy flux of ingress and egress through the control surface are in equilibrium state during the ablation process. The mass conservation constructs the correlation of material loss, material property, and working condition. Table 2 and Table 3 show the mechanical and thermal properties of C/C composites, respectively. The energy conservation indicates the heat transfer during the ablation

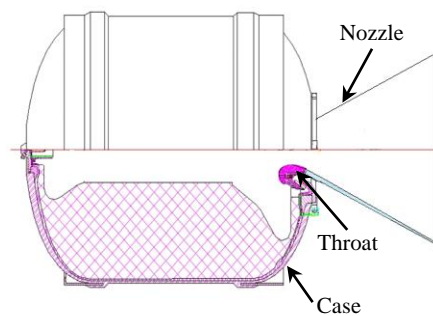


Fig.3 Schematic diagram of SRM

Table 1 Parameters of C/C composite throats for SRM tests

Specimen	Ablation duration/s	Throat dimension, Φ_{out}/Φ_{in}
1	20	60 mm/20 mm
2	60	300 mm/120 mm
3	95	300 mm/120 mm

Table 2 Mechanical properties of C/C composites

Parameter	Direction	Strength/MPa	Modulus/GPa	Strain/%
Tensile	x-y	185	72.10	0.11
	z	131	57.70	0.18
Compress	x-y	136	7.31	2.60
	z	195	4.22	6.50

process. The general mass conservation, specimen conservation, and energy conservation laws at the gas-solid interface can be expressed as Eq.(2-4), respectively:

$$\bar{\rho}_g u_r = \rho_c r_c \quad (2)$$

$$\left(-\bar{\rho}_g D_{km} \frac{dY_k}{dr} + \bar{\rho}_g Y_k u_r \right)_r = \bar{\omega}_k \quad (3)$$

$$\lambda_c \left(\frac{\partial T}{\partial r} \right)_c + k_c \rho_c h_c = \lambda_g \left(\frac{\partial T}{\partial r} \right)_g + \sum_{k=1}^N \bar{\omega}_k h_{g,k} \quad (4)$$

where $\bar{\rho}_g$ is the gas density due to throat ablation; ρ_c is the C/C density; u_r is the gas mass flux; r is the linear ablation rate; $\bar{\omega}_k$ is the mass production rate of k species; D_{km} and Y_k are the reactant diffusion coefficient and mass fraction of k species, respectively; λ is the thermal conductivity; h is the constituent enthalpy; T is the temperature; the subscripts g and c represent the gas and C/C composites, respectively; k is the production species of gas-phase at the throat surface.

2.1.2 Convective heat transfer coefficient

The convective heat transfer coefficient was calculated by Bartz equation under the condition of hot gas at 3500 K, and the radiation heat transfer was negligible. The throat has the constant profile during the ablation process. Fig.4 shows the convective heat transfer coefficients of C/C composite throat surface of different specimens during the ablation process. The heat transfer coefficient increases gradually from the

convergent zone to the central throat zone until the maximum convective heat transfer coefficient is achieved at the central throat zone. Then the heat transfer coefficient gradually decreases in the throat exit zone. Therefore, the convective heat transfer is related to the gas pressure, mass flux, and the throat profile. The high heat transfer results in the high surface temperature.

2.1.3 Temperature distribution

The throat temperature is a major influencing factor in ablation, because it directly affects the reactivity between the throat and the oxidants in the combustion gas. Numerical simulations were conducted to obtain the temperature distribution in the throat. The wall temperature was calculated based on the surface energy equilibrium, which is related to the gas temperature, convective heat transfer coefficient, and the thermal properties of C/C composites. The outer adiabatic wall condition was enforced; therefore the throat contour was regarded as a constant during the ablation. Fig.5 shows the simulation of temperature distribution in the interior throat. Fig.6 shows the relationship between the axial gas temperature and distance of the throat inner wall surface. The maximum temperature zone of the throat is the throat convergent zone. The maximum temperature of Specimen 3 is about 3360 K at the input region of throat, then the temperature drops to about 2900 K at the center region, and finally that at the surface of exit edge decreases to 2500 K. There is a temperature platform at downstream of the central throat zone. The external wall of the throat has the lowest temperature.

2.1.4 Axial stress distribution

Fig.7 shows the axial stress distributions of the interior zone in C/C composite throat. The maximum stress of Specimen 1 is obtained at the input region of throat, because

Table 3 Thermal properties of C/C composites

Parameter	Direction	RT	1273 K
Thermal conductivity/ $W \cdot m^{-1} \cdot K^{-1}$	x-y	150	85
	z	94	63
Specific heat at constant pressure, $C_p/J \cdot kg^{-1} \cdot K^{-1}$	x-y/z	965	2460
Coefficient of thermal expansion/ $\times 10^{-6}$	x-y	-0.595	1.013
	z	-0.397	1.387

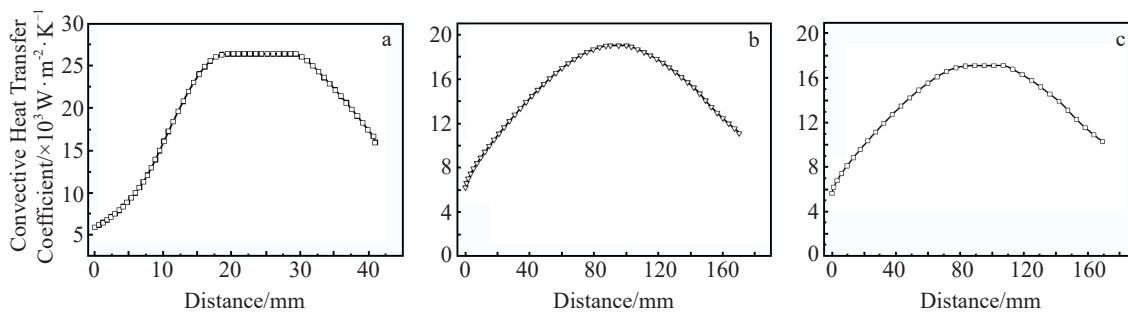


Fig.4 Convective heat transfer coefficients of C/C composite throat surface of different specimens in ablation: (a) Specimen 1; (b) Specimen 2; (c) Specimen 3

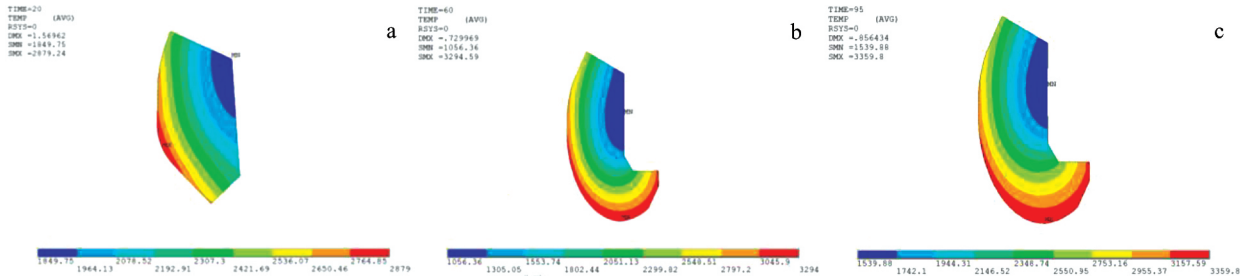


Fig.5 Temperature distributions of throat interior zone of Specimen 1 (a), Specimen 2 (b), and Specimen 3 (c)

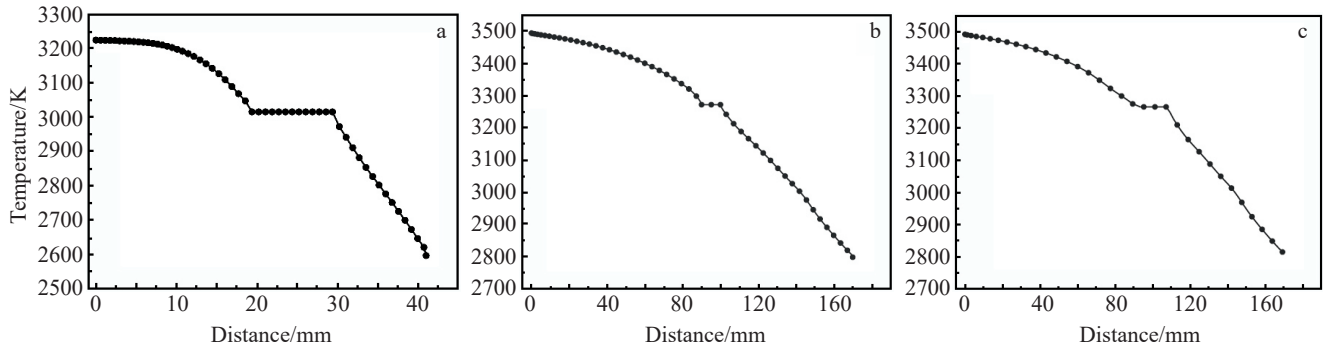


Fig.6 Axial gas temperature distributions at inner wall surface of Specimen 1 (a), Specimen 2 (b), and Specimen 3 (c)

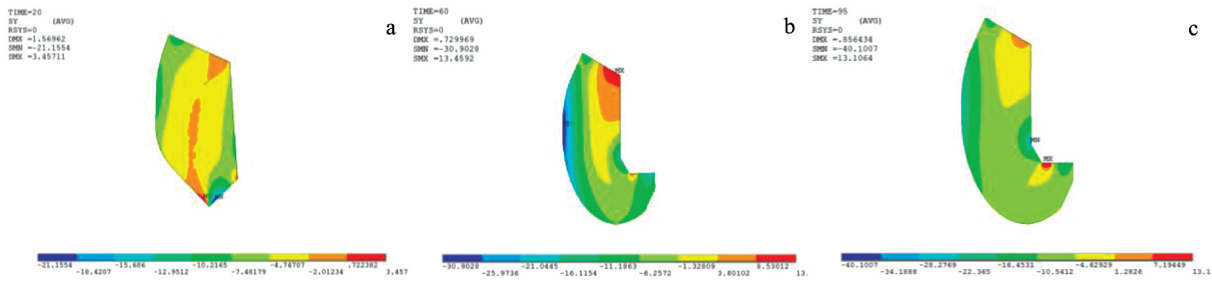


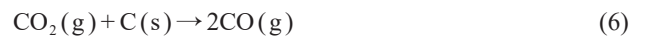
Fig.7 Axial stress distributions of Specimen 1 (a), Specimen 2 (b), and Specimen 3 (c)

there is a sharp tip. The maximum stress of Specimen 2 is about 30 MPa at central throat zone, which corresponds to the convective heat transfer and the temperature gradient between the inner and outer surfaces. The stress distribution of Specimen 3 is similar to that of Specimen 2, because of their same sizes and similar simulation conditions. The stress decreases from the inner surface to the external wall, so the central throat zone bears the maximum mechanical load during ablation process.

2.1.5 Gas products calculation

The mole fractions of equilibrium combustion components were calculated by the chemical equilibrium with applications^[23,24] based on the free-energy-minimization principle. The content of components in the combustion products are presented in Table 4, which remains nearly constant at the pressure of 6.5 MPa for different specimens. The results show that the combustion products consist of H₂O, CO₂, CO, H₂, N₂, HCl, and Al₂O₃/Al particles. The oxidizing components, such as water (H₂O), carbon dioxide (CO₂), and

hydrogen (H₂), are the primary reactants with the carbon in the throat ablation process^[25]. The reactions are expressed as follows:



2.2 Ablation behavior

2.2.1 Ablation rate

The throat surface is equally divided into three zones based on the contour, temperature distribution, and stress distribution: convergent zone, central zone, and divergent zone, as shown in Fig. 8. The average linear ablation rate was

Table 4 Components of SRM combustion

Component	H ₂ O	CO ₂	CO	H ₂	N ₂	HCl	Al ₂ O ₃ / Al
Mass fraction/wt%	18.12	7.74	30.12	1.69	8.97	22.50	10.86
Mole fraction/mol%	24.29	4.25	25.95	20.38	7.72	14.86	2.55

calculated based on rate of the initial and final throat central zone diameters.

Fig.9 shows the pressure-time curve of Specimen 1 during ablation process. The end of combustion process is determined by the decline in smooth exponential of the pressure-time curve. The decline point usually lies beyond the abrupt pressure drop of the quasi-steady portion of the curve. There is a rapid rise in pressure during the ignition transient interval. Fig. 10 shows the similar appearances of C/C composite throats after ablation. It is clear that the inner wall has smooth surface without grooves or cracks. Specimen 2 and Specimen 3 are dissected. Fig.11 shows the contours of C/C composite throats before and after ablation. The linear ablation rate of the throat is increased from the input zone and reaches the maximum value at the central throat region, which exhibits the similar trend with the temperature distribution in Fig.5. The temperature of the inner throat surface can decide

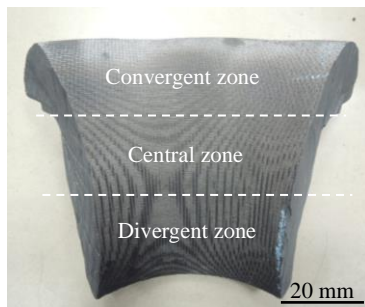


Fig.8 Different zones of C/C throat

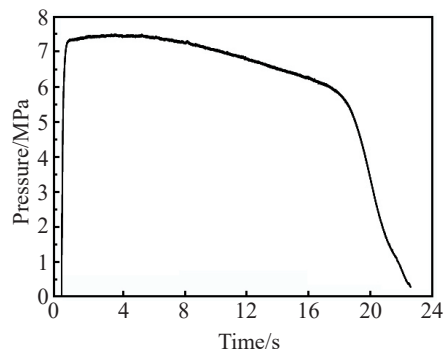


Fig.9 Relationship of pressure-time of Specimen 1 during ablation

the reaction rate, which has an importance effect on the ablation behavior. The average linear ablation rate of different specimens is listed in Table 5, which is 0.063~0.164 mm/s, and the maximum ablation rate is 0.164 mm/s for Specimen 3.

2.2.2 Ablation morphology

(1) Convergent zone

The morphologies of inner throat surface at different scales were analyzed by SEM and energy dispersive spectroscopy (EDS), as shown in Fig.12. Fig.12a shows a relatively smooth mesh surface with many micro-pits of Specimen 2. The carbon fiber yarns are ruptured and the matrix remains. The contour of the C/C composite throat does not change before and after ablation. The mesh hole is the ablated carbon fiber yarns, and there are lots of grooves on the surface. Fig. 12b shows a rough and porous ablated surface. The carbon fiber yarns (Fig.12c) exhibit “pencil tip” morphology, and they are severely ablated. The carbon matrix is less ablated than the carbon fiber yarn. However, the rough surface and pits can still be found, compared with the original C/C composite throat. The other two specimens show the similar morphologies of carbon fiber yarn and the carbon matrix.

Temperature and the content of oxidation components near the surface are two important parameters affecting the chemical ablation. At the transient ignition of SRM, the high temperature combustion gas mainly heats the throat by convection heat transfer, and the throat reaches the heat equilibrium instantaneously^[7]. The calculated temperature of convergent zone is much higher than that of other zones, because the combustion gas is assembled in convergent zone. The higher the temperature rise, the quicker the chemical reactions. The content of oxidation components near the surface severely influences the ablation rate. The cross-flow mass flux is linked with the Reynolds number based on the throat contour. The thickness of boundary layer is another important parameter, which refers to the local shear stress at the throat station. The combustion pressure has little effect on the gradient distribution of gas^[25]. So the diffusion of oxidants to the throat surface is the restriction factor of the ablation. The ablation at the convergent zone is the diffusion-controlled thermochemical ablation.

(2) Central zone

Fig. 13 shows the morphologies of central throat zone, which present obviously rougher surface, compared with

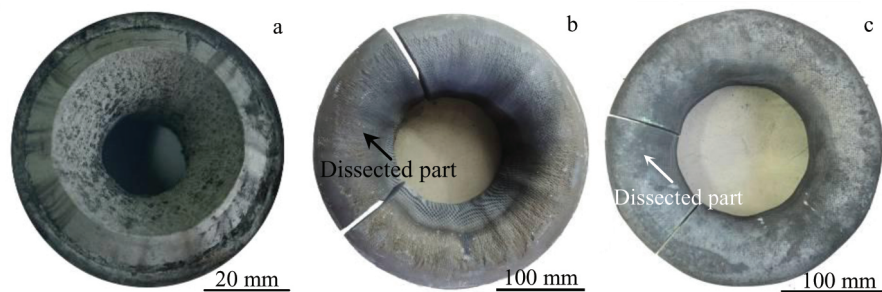


Fig.10 Appearances of C/C composite throats of Specimen 1 (a), Specimen 2 (b), and Specimen 3 (c)

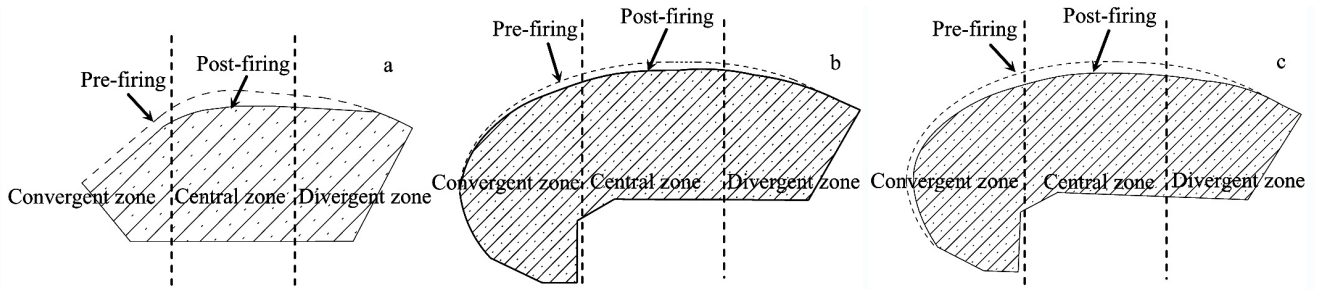


Fig.11 Contours of Specimen 1 (a), Specimen 2 (b), and Specimen 3 (c) at pre-firing and post-firing states

Table 5 Ablation results of C/C composite throats of SRM

Specimen	Average linear ablation rate/mm·s ⁻¹	Maximum ablation depth/mm
1	0.063	1.36
2	0.138	8.64
3	0.164	15.96

those of the original surface. The carbon fiber is ablated to needle-tip shape. There are lots of voids and grooves on the surface. The throat surface becomes relaxation, and the defects are formed by the axial stress (Fig.7). The ablation is affected by these defects which facilitate the thermochemical ablation onto the throat with inner structural integrity by oxidation components (H₂O, H₂, and CO₂). The heterogeneous reactions of the gaseous components with carbon in the throat result in fast ablation rate^[26].

The high temperature exhaust gas is accelerated by the high pressure in the central zone, the speed of which may reach the

sonic velocity. The high-speed gas flow produces a swirling flow through the throat, because the tangential velocity cannot be neglected. The swirl velocity affects the denudation ablation in the central zone. The mechanical denudation occurs in the 3D C/C composite. The mechanical properties of C/C composite throat decrease during SRM running. The particle or block denudation results from the defects, so it is thermal-mechanical coupling ablation. In addition, the content of high-speed melting Al₂O₃/Al is the largest in the central throat zone^[27]. The probability of particle collision on the surface becomes large, which is related to the partial pressure proportional to the mass fraction of components and the mixture density. The tip temperature increases when the particle collision occurs on the surface, because the particles possess thermal energy and kinetic energy to heat the tip. Thus, the thermochemical ablation is aggravated at the particle points. The particle erosion may also be aggravated due to the impingement of the condensed Al₂O₃ particles with high kinetic energy on the throat surface. Therefore, the C/C

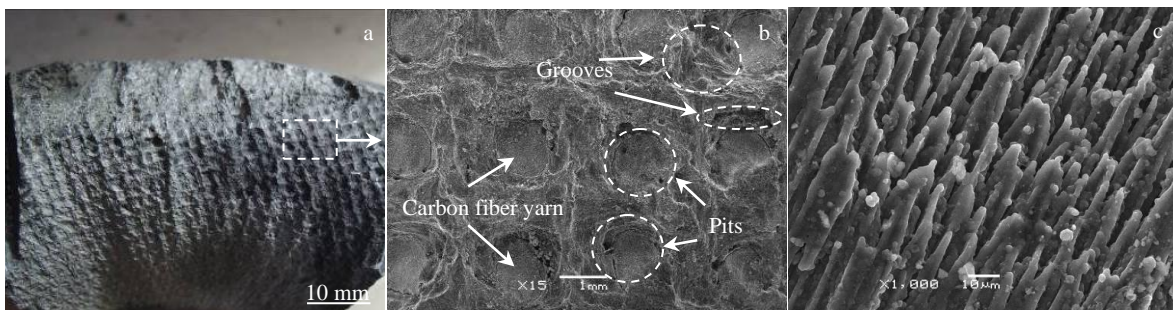


Fig.12 Morphologies of convergent zone of Specimen 2 at different scales: (a) macro-scale; (b) meso-scale; (c) micro-scale

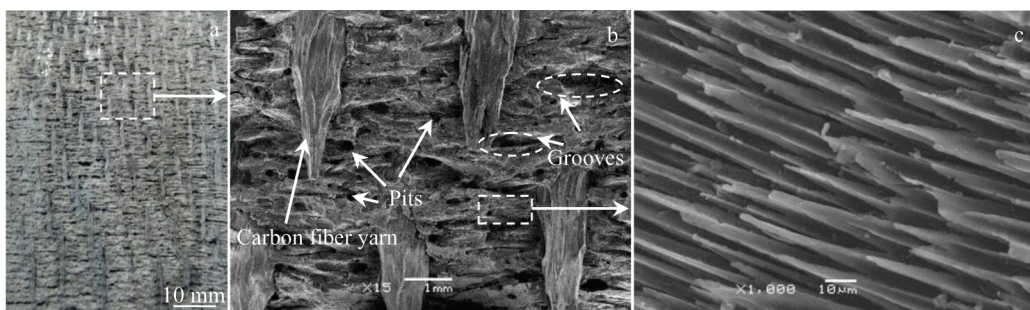


Fig.13 Morphologies of central throat zone at different scales: (a) macro-scale; (b) meso-scale; (c) micro-scale

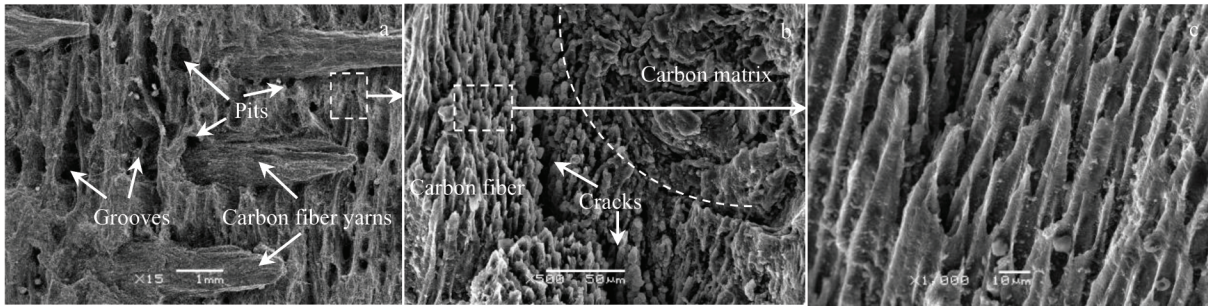


Fig.14 Morphologies of divergent zone at different scales: (a) macro-scale; (b) meso-scale; (c) micro-scale

composite structure is broken and the mechanical properties of the throat are reduced. In general, the ablation mechanism of the central throat zone is the combination effect of thermochemical ablation, mechanical denudation, and particle erosion.

(3) Divergent zone

Fig. 14 shows the morphologies of divergent zone of C/C composite throat surface after ablation. The carbon fiber is ablated to needle-tip shape. Many cracks appear on the carbon fiber and the interface between the carbon fiber and matrix due to the mismatch of thermal expansion between carbon fiber and matrix. There are lots of pits and grooves on the surface because of the heterogeneous reactions at high temperature. The divergent zone is conical with a divergence cone angle of 30° . The gas axial velocity increases at the downstream of the central zone, and reaches the supersonic at the throat exit, due to the flow expansion caused by the divergent geometry. Both the temperature and content of oxidation components decrease largely in the divergent zone near the surface, compared with those at the upstream. Besides, the surface stress also declines. The reduction in ablation rate is attributed to the decreased contents of H_2O , CO_2 , and Al_2O_3/Al and the reduced temperature in the divergent region. The ablation process may be influenced by the diffusion of oxidation components through the turbulent transport from the core region across the boundary layer to the throat surface. The turbulence level is generally governed by the Reynolds number at the throat region.

(4) Special morphology

Fig. 15 shows the morphology of Al_2O_3 ball formed in the divergent region on throat surface after ablation. The elements of Al_2O_3 ball were detected by EDS. Lots of balls of $1\sim 3\ \mu m$ in diameter adhere to the ablated carbon fiber. This specific morphology is caused by gas at ending part of ablation. The appearance of Al_2O_3 balls is due to the propellant containing 18wt% Al particles. The fused Al_2O_3 droplets were deposited on cold throat surface, and then they were cooled down, forming the Al_2O_3 ball.

Fig. 16 shows the morphology of pyrolysis carbon layer in the divergent zone of the throat surface. The pyrolysis carbon layer covers the ablated carbon fiber due to the combustion gaseous reactants which contain alkane (carbon precursor). At the ending part of ablation, the inner chamber of throat

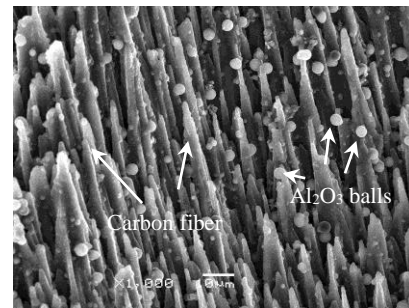


Fig.15 Morphology of Al_2O_3 balls on carbon fiber on throat surface

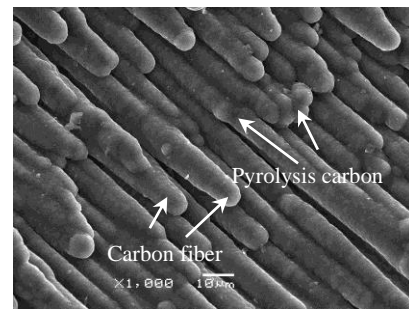


Fig.16 Morphology of pyrolysis carbon layer on throat surface

becomes a small tube furnace with appropriate temperature and proper reactant gas flow. The heating is provided by the C/C composite throat because of its high heat storage capacity. The chemical deposition or adsorption of carbon on the throat surface occurs. No pyrolysis carbon can be found at the central throat zone, indicating that the deposition does not occur during the ablation. This phenomenon is beneficial for the throat ablation, because the deposition vapor may consume the flame heat.

3 Conclusions

- 1) The average linear ablation rate of the carbon/carbon (C/C) composite throat is $0.063\sim 0.164\ \text{mm/s}$ for the solid rocket motor.
- 2) The temperature reaches the maximum value at the convergent zone of throat inner surface, and the exhaust gas oxidation components cause the thermochemical ablation.
- 3) In the central throat zone, the temperature and stress

have effect on the ablation behavior of C/C composite throat. The throat structural integrity is broken due to the thermal oxidation and stress. Mechanical denudation is the main ablation mechanism in the central throat zone.

4) The Al_2O_3 drops result in particle erosion. The ablation rate is decreased with decreasing the temperature and stress in the divergent zone. The ablation mechanism is the combination effect of the thermochemical ablation, mechanical denudation, and particle erosion.

References

- Maisonneuve Y. *Aerospace Science Technology*[J], 1997, 1(4): 277
- Meng S H, Zhou Y J, Xie W H et al. *Journal of Spacecraft and Rockets*[J], 2016, 53(5): 930
- Wang Liwu, Tian Weiping, Guo Yunqiang et al. *Journal of Solid Rocket Technology*[J], 2019, 42(2): 135 (in Chinese)
- Turchi A, Bianchi D, Nasuti F et al. *Aerospace Science and Technology*[J], 2013, 27(1): 25
- Vignoles G L, Lachaud J, Aspa Y. *Environmental Effects: Ablation of C/C Materials-Surface Dynamics and Effective Reactivity*[M]. Hoboken: Wiley & American Ceramic Society, 2014: 353
- Cavallini E, Bianchi D, Favini B et al. *47th AIAA/ASME/SAE/ASEE Joint Propulsion Conference & Exhibit*[C]. San Diego: American Institute of Aeronautics and Astronautics, 2011: 5799
- Su Junming, Zhou Shaojian, Xue Ningjuan et al. *New Carbon Materials*[J], 2018, 33(5): 442 (in Chinese)
- Fitzer E, Manocha L M. *Carbon Reinforcements and Carbon-Carbon Composites*[M]. Berlin: Springer-Verlag, 1998: 241
- Thakre P, Yang V. *Journal of Propulsion and Power*[J], 2008, 24(4): 822
- Yao X Y, Chen M M, Feng G H. *Rare Metal Materials and Engineering*[J], 2020, 49(1): 241
- Li Hejun, Shi Xiaohong, Shen Qingliang et al. *The Chinese Journal of Nonferrous Metals*[J], 2019, 29(9): 2142 (in Chinese)
- Kumar R R, Vinod G, Renjith S et al. *Materials Science & Engineering A*[J], 2005, 412(1-2): 66
- Alain L, Thierry P, Marc L. *43rd AIAA/ASME/SAE/ASEE Joint Propulsion Conference & Exhibit*[C]. Cincinnati: American Institute of Aeronautics and Astronautics, 2007: 5470
- Yin J, Xiong X, Zhang H B et al. *Carbon*[J], 2006, 49(9): 1690
- Li W J, Huang H M, Hu Y M. *Thermal Science*[J], 2014, 18(5): 1625
- Zhang B, Li X D. *Applied Composite Materials*[J], 2017, 25(1): 191
- Gillard A P, Couégnat G, Chupin S et al. *Carbon*[J], 2019, 154: 178
- Zha B L, Su Q D, Shi Y A et al. *4th International Conference on Applied Materials and Manufacturing Technology*[C]. Nanchang: IOP Publishing, 2018: 710
- Lachaud J, Aspa Y, Vignoles G L. *International Journal of Heat and Mass Transfer*[J], 2008, 51(9-10): 2614
- Li Q, Li J, He G Q et al. *Carbon*[J], 2014, 67: 140
- Lachaud J, Aspa Y, Vignoles G L. *International Journal of Heat and Mass Transfer*[J], 2017, 115(A): 1150
- Chen B, Zhang L T, Cheng L F et al. *Carbon*[J], 2009, 47(3): 545
- Gordon S, McBride B J. *NASA Report*, NASA RP-1311[R]. Cleveland: NASA Lewis Research Center, 1994
- Gordon S, McBride B J. *NASA Report*, NASA RP-1311-P2[R]. Cleveland: NASA Lewis Research Center, 1996
- Vignoles G L, Aspa Y, Quintard M. *Composites Science and Technology*[J], 2010, 70(9): 1303
- Kamps L, Saito Y, Kawabata R et al. *Journal of Propulsion and Power*[J], 2017, 33(6): 1
- Bianchi D, Nasuti F, Onofri M et al. *Journal of Propulsion and Power*[J], 2011, 27(1): 197

固体火箭发动机3D C/C材料喉衬热结构模拟与烧蚀行为

王富强^{1,2}, 陈建¹, 王坤杰², 崔红², 嵇阿琳², 谢栋², 白杨²

(1. 西安工业大学材料与化工学院, 陕西 西安 710021)

(2. 西安航天复合材料研究所, 陕西 西安 710025)

摘要: 以高氯酸铵/端羟基聚丁二烯/Al三组元为推进剂, 在压强6.5 MPa、工作时间20、60、95 s的烧蚀条件下, 进行长时间的固体火箭发动机烧蚀, 模拟计算了喷管3D C/C材料喉衬热平衡状态下的对流换热系数、温度场和应力场, 结合计算结果分析了喉衬各区的烧蚀特征与机理。结果表明: 喉衬收敛段温度最高, 烧蚀为氧化组分(H_2O 、 CO_2 、 H_2)与表面碳发生的热化学烧蚀; 喉径区换热系数最大, 温度较高, 内表面在应力作用下, 烧蚀最为严重, 为燃气热化学烧蚀、高速气流机械剥蚀及粒子冲刷的共同作用, 表面呈现出微小的沟槽或裂纹, 应力与氧化使喉衬在低于材料极限应力下发生分解破坏; 出口段应力降低, 温度明显下降, 烧蚀率显著降低。喉衬烧蚀机理为温度、应力影响下燃气氧化组分与碳的热化学烧蚀、气流机械剥蚀和 Al_2O_3 颗粒侵蚀的联合作用。

关键词: 喉衬; 热结构模拟; 烧蚀行为; C/C; 固体火箭发动机

作者简介: 王富强, 男, 1981年生, 博士生, 高级工程师, 西安工业大学材料与化工学院, 陕西 西安 710021, 电话: 029-83601105, E-mail: shiyanshi050428@163.com